

# CHAPTER 7

## High energy emission from galactic jets<sup>1</sup>

H. R. Christiansen

*Physics Department, State University of Ceara, Av. Paranjana 1700, Fortaleza - CE, Brazil*

**Abstract.** In this chapter we review some aspects of X-ray binaries, particularly those presenting steady jets, i.e. microquasars. Because of their proximity and similarities with active galactic nuclei (AGN), galactic jet sources are unique laboratories to test astrophysical theories of a universal scope. Due to recent observational progress made with the new generation of gamma-ray imaging atmospheric Cherenkov telescopes and in view of the upcoming km<sup>3</sup>-size neutrino detectors, we focus especially on the possible high-energy gamma radiation and neutrino emission. In connection with this, we also comment about astrophysical jets present in young stellar objects, and we briefly discuss similarities and differences with extragalactic AGN and gamma-ray bursters.

**Keywords:** jets, X-ray binaries, microquasars, neutrinos, gamma-rays

**PACS:** 98.58.Fd Jets, outflows and bipolar flows. 98.70.Rz Cosmic gamma-ray sources; gamma-ray bursts. 97.80.Jp X-ray binaries. 95.85.Ry Neutrino, muon, pion, and other elementary particles; cosmic rays.

## INTRODUCTION

Astrophysical jets are collimated outflows that seem to occur wherever accretion of matter with angular momentum in a gravitational potential takes place. The presence of magnetic fields probably plays a major role in the formation and launching of such jets. They are observed over a wide range of spatial scales, from AGN to protostars.

Binary systems with jets offer two great advantages as potential natural laboratories for the investigation of astrophysical outflows: they can be found at relatively short distances from the Solar System and the mechanisms involved in the production of the observed phenomenology operate on relatively short time scales. A variety of microscopic processes due to electromagnetic, weak and strong interactions in the jets of such systems result in the production of radiation covering the whole spectrum, yielding a unique source of information on the associated physics. Ground-based and satellite detectors can measure this radiation and probe the innermost regions of the sources as well as the interaction of the jets with the environment.

There is clear evidence of the presence of relativistic leptons in galactic jets: extended non-thermal emission and polarization can be measured in radio-wavelengths and, in

---

<sup>1</sup> Published by Cambridge Scientific Publishers (CSP) in *The Sun, the Stars, the Universe and General Relativity*, Cambridge 2011. ISBN 978-1-908106-12-4

some cases, up to X-rays. The presence of an accretion disc of baryonic matter and the detection of very high energy (VHE) emission strongly supports a hadronic jet's content as well (e.g. [1, 2]).

Relativistic electrons in the jets suffer synchrotron and inverse Compton losses. In cases where strong photon fields from the donor star are present, complex processes like electromagnetic cascading can take place (e.g. [3, 4]). In addition, the likely hadronic content of some jets should also result in energetic neutrinos together with VHE gamma-ray production. Indeed, relativistic  $pp$  and  $p\gamma$  collisions give rise to very energetic pions rapidly decaying into leptons and gamma-rays. Remarkably, muon-neutrinos above 1 TeV from this type of sources will be detectable with ICECUBE in the near future, opening a new era in astronomy (see e.g. [5] and Neutrino section, below).

In the understanding of VHE emitting sources, cooling and accelerating hadron processes are crucial to evaluate the final maximum proton energies available in the acceleration region. Considering that the fractional power of ultra-relativistic protons can be determined by means of the most restrictive observational data, the local steady distribution of parent pions and the resulting gamma-rays and neutrino fluxes can be theoretically predicted [6]. Current and upcoming experiments such as MAGIC II, VERITAS, HESS II, CTA and GLAST should shed strong light on most of these issues in the next few years.

In what follows we review and highlight some topical issues in this fast-developing field.

## GALACTIC X-RAY BINARIES

X-ray binaries (XRBs) contain a stellar mass compact object (CO) (white dwarfs have been excluded) which is supposed to emit X-rays as a consequence of gravitational accretion of matter from the companion. The companion, also known as donor, is a non-degenerated star which can be in any stage of its evolution.

As of 2007, the hitherto last catalogue of low (donor) mass XRB (LMXB) in the galaxy signals the identification of 185 of such systems (excluding quiescent systems) [7]. The related catalogue for high mass XRBs (HMXB) indicates 114 of these binaries [8]. LMXB are formed by a black hole or neutron star with a late-type main sequence star (A, F, G) or even a white dwarf. Typical LMXB secondaries have masses below  $1M_{\odot}$  and are Roche-lobe deformed by the compact object. HMXB comprise an OB donor (Be or SG type) and a black hole or neutron star. Note however that black holes and Be stars are not found together.

About 20% of the three hundred XRBs catalogued, 56 LMXB and 9 HMXBs, are seen as clear radio emitting sources of which at least 15, and possibly up to 20, can be already enlisted in the microquasar category. Microquasars are rapidly variable X-ray binaries that present extended jets strongly emitting in radio and, in some cases, up to X-rays and even higher energies. It is supposed that the compact object magnetically powers a relativistic jet via accretion of matter from the companion.

So far, the only well established VHE (TeV) gamma-ray emitters are 4 galactic HMXBs (PSR B1259-63, LS I+61 303, LS 5039, Cyg X-1), the first of which harbors a non-accreting pulsar while the last one holds an accreting black hole. The nature of

the compact components of the other two systems is not completely established since their masses are just roughly known ( $1 - 5 M_{\odot}$ ), but they are likely to belong to the microquasar category. Note also that there is an equivalent number of already confirmed XRBs (particularly HMXB) in the Magellanic Clouds that might be similar to the galactic ones in every sense. In any case, the number of objects of each class mentioned above will, presumably, be increasing as fast as new technologies get incorporated among the detection facilities.

## X-ray signature, accretion and spectral states

Most of the present understanding about jets in XRBs comes from the study of black hole (BH) candidates. The main reason is that they are more easily detected since, in general, BH XRBs are more radio loud than neutron star (NS) XRBs.

Accreting black holes though emit most of their luminosity in the X-ray band, which strongly varies depending on the accretion state of the source. Indeed, the same source can exhibit very different X-ray spectra characterizing a diversity of XRB spectral states. There are two main such states relatively steady and frequently observed. At high luminosities (above  $\sim 0.1$  of the Eddington luminosity <sup>2</sup>), it is said that the accretion flow is in the High Soft State (HSS), characterized by a strong (*high*) thermal disc radiation and some reflection contributions likely associated with illumination between the accretion disc and the corona. It also presents a weak (*soft*) non-thermal (power-law) component extending up to high energies (X-rays and low energy  $\gamma$ -rays). This power-law, with a steep photon index  $\sim 2.3-2.5$ , is interpreted as coming from inverse Compton (IC) upscattering of UV and soft X-ray photons by thermal ( $kT \simeq 30 - 50$  keV) and non-thermal (index  $\sim 3.5-4.5$ ) electrons of a hot plasma or corona (see e.g. [9]). This non-thermal comptonization on top of a black body spectrum peaking around 1 keV strongly characterizes the HSS.

At *low* luminosities (below a few percent of  $L_{\text{Edd}}$ ) the sources are mostly found in the so-called Low Hard State (LHS) in which disc blackbody features and reflection properties are weak. There seems to be a hot corona dominating the luminosity output of the system and emitting a thermal distribution of electrons that boost (*harden*) the energy of X-rays [10]. LHS spectra are very well fitted by multiple Compton up-scattering of soft photons by a Maxwellian distribution of electrons (see [11]) in a hot plasma ( $kT \simeq 50 - 100$  keV). It is this thermally comptonized spectrum, dominated by a hard power-law (index  $\sim 1.5-1.9$ ) with an exponential cutoff around 100 keV, that characterizes the LHS.

Besides the LHS and HSS, there are several other intermediate states (IMS) more difficult to define, often appearing when the source is about switching between the two main states. For example, the rapid X-ray transition from hard to soft states is associated with radio flares which show optically thin spectra in a steep power-law state also known as very high (VHS). These flares are signatures of powerful ejection events,

---

<sup>2</sup>  $L_{\text{Edd}} \simeq 10^{38} M/M_{\odot}$  erg/s, where  $M$  is the mass of the accreting object.

spatially resolved as large-scale extended jets. Intermediate states are easily identified in hardness-intensity diagrams (HID), which present a typical hysteresis or q-like form along the different spectral states. They have been used with great success to study the evolution of outbursts and to distinguish the different accretion states of a source (e.g. [12, 13, 14]), in particular the radio-loud and radio-quiet phases. In addition, the timing properties of the X-ray light curve change dramatically with the position in the HID (e.g. [12, 15]).

The different spectral states are usually understood in terms of changes in the geometry of the accretion flow. The standard picture (e.g. [16]) is that in the HSS there is a geometrically thin disc extending down to the last stable orbit. This disc is responsible for the (dominant) thermal emission and is the source of soft photons for later comptonisation in small active coronal regions located near the disc. There, electrons absorb energy through magnetic reconnection/dissipation processes [17]. These electrons thereafter lose energy by boosting the soft photons coming from the disc. This produces a high energy non-thermal emission which, in turn, illuminates the disc inducing reflection features in the source [18]. When the system is steadily in the soft state, there is a quenching in radio emission which may be due to the physical suppression of the collimated outflow [19].

In the standard model of spectral states, the LHS is explained by means of a truncated geometrically thin disc [20]. Instead of extending down to the last stable orbit, this disc is terminated at large distances that range from a few hundred to a few thousand gravitational radii from the black hole as suggested by the weakness of its thermal features. In the inner parts, the accretion flow takes the form of a hot geometrically thick, optically thin, corona-like structure [21, 22], possibly advection dominated and radiatively inefficient [23]. The electrons have a thermal distribution that can cool down by comptonisation of the soft photons coming from the external geometrically thin disc and IR-optical photons internally generated through self-absorbed synchrotron radiation. See also [24, 25]. In the LHS, the observed radio emission is optically thick with a flat or slightly inverted spectrum, and indirect evidence indicates that this is the signature of a continuous outflow or compact jet [26].

For BH XRBs in the hard state, it has been found a non-linear correlation between the radio and the X-ray luminosities. It runs over more than three orders of magnitude in the X-ray band and reads  $L_R \propto L_X^{0.7}$  [27, 28]. Remarkably, extending this correlation to supermassive BHs, there is evidence that a single 3D power-law function can fit all the BH data (XRBs and AGN) for a given X-ray luminosity, radio luminosity and CO mass. This function takes the approximate form  $L_R \propto L_X^{0.6} M^{0.8}$  where  $M$  is the mass of the compact object [29, 30]. The existence of this relation, connecting BH XRBs and AGN, signals that the same physical processes could be responsible for the disc-jet coupling, irrespective of the mass of the BH involved [31]. In a separate section, we shall come again to the description of the spectral relations in the case of NS XRBs.

## GALACTIC JETS

The study of XRBs at different wavelengths has shown that a significant fraction of the accretion power may be released in the form of radiatively inefficient collimated out-

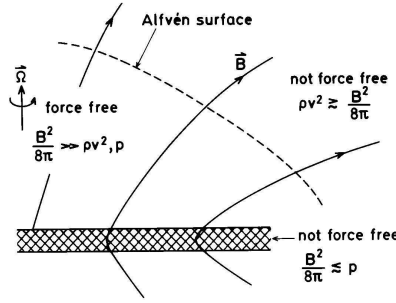


**FIGURE 1.** Regions in a magnetically accelerated flow from an accretion disc. The central object is assumed at the left of the sketch. Figure from [36].

flows or jets. In general, jets are a very common feature associated with accretion onto relativistic compact objects on all mass scales, from neutron stars and stellar mass black holes in XRB systems to supermassive BHs in active galactic nuclei. Strong jets are believed to be even at the origin of gamma-ray bursts, the most overwhelming transient events ever detected, but seen as well among young stellar systems (see separate section below). The investigation of the link between the jet emission and the different accretion regimes of an astrophysical system is an important issue which can explain much on its internal dynamics.

Galactic jets from binary systems are particularly interesting because they develop completely in short time scales and, in many cases, we are able to survey the whole cycle of their existence. During the LHS, radio emission from XRBs points towards the presence of a persistent jet in some of these systems, and transient ejections also seem to take place when spectral states switch from the LHS to the HSS.

Depending on the object, the nonthermal radiation produced in XRB jets has been resolved in radio at very different spatial scales but also in X-rays at large scales (see e.g. [32]). This is clear evidence that particle acceleration takes place in different locations of XRB jets under very different conditions (for a discussion see e.g. [33]).

## Launching and powering

Although a complete theory of jet generation is still lacking, several studies of jet powering, acceleration, and collimation have been carried out during the last few decades (e.g. [34, 35]). Due to the observed correlation between accretion and jet activity in this kind of system (see e.g. [13]), a widely accepted scenario suggests that jets are powered and fed by gravitationally driven accretion. Under certain conditions, magneto-centrifugal forces make the matter of the accretion disc move following ordered magnetic field lines that thread the inner regions of the disc.

As explained in [36], outflows are produced by magnetic field lines anchored in the material of a rapidly rotating object. Indeed, numerical simulations show that an ordered magnetic field near the central object operates upon the ejection of powerful outflows.

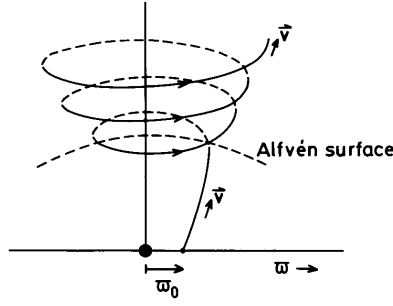


**FIGURE 2.** Magnetic field lines and particle path in the outflow.  $\bar{\omega}$  is the orthogonal distance from the compact object. Figure from [36].

In the standard magneto-centrifugal acceleration model for jets produced by an accretion disc [37, 38] three different regions can be distinguished [36]: (i) The accretion disc itself, where the kinetic energy density dominates over the magnetic one and makes the field lines corotate with the disc. (ii) An atmosphere of plasma extending outside the disc which, assuming it is cool, has a low density and pressure. The gas is therefore dominated by the magnetic pressure which then drives the flow into corotation. The velocity component along the field is though unrestricted and the centrifugal force accelerates the gas along the field lines. Consequently, bulk-matter loading and acceleration depend on the inclination of the field lines and a net upward force acts only if they are sufficiently inclined outward [38]. It implies that the conditions for acceleration and collimation (i.e. the degree to which the jet flow lines are parallel) are rather opposed so that highly collimated jets would require further explanation. In addition, note that for a given field shape the mass loading decreases with increasing field strength [39]. (iii) Near the Alfvén radius (i.e. the distance from the CO where the *ram* pressure equals the magnetic pressure) the rigid corotation approximation breaks down. While the flow accelerates with the increasing inclination of the field lines, the field strength decreases with distance (see Model section). The velocity of the bulk is very high and the matter flow starts separating from the field lines. Its rotation rate gradually vanishes in order to conserve angular momentum as the flow continues to expand away from the axis. On the other hand, in this region the field lines become nearly azimuthal, at least in a pure axisymmetric model.

After launching, the flow is first accelerated by the centrifugal effect up to a distance of the order of the Alfvén radius. When the temperature in this region is high, for example in the presence of a hot corona, the atmosphere extends higher on and it is easier for the mass flow to get started. If the disc atmosphere is cool (well below the virial temperature), the gas density declines rapidly with height and the mass flow rate becomes more sensitive to the physical conditions near the disc surface. In the radial direction, the flow velocity increases almost linearly with distance (from the rotation axis) up to the magnetosonic speed ( $\simeq$  sound speed  $c_s$ ), and thus the mass flow rate attains the value  $\dot{m} \simeq c_s \rho_s$ , where  $\rho_s$  is the gas density at the maximal velocity.

The matter contents of the jets are not exactly known, but the presence of relativistic

hadrons in the jets of SS 433 has been directly inferred from iron X-ray line observations (e.g. [40, 41, 42]). In addition, the large deformations that some jets induce in the interstellar medium suggest a significant baryon load [43, 44]. The fact that the jets are usually well collimated also favors this interpretation since cold protons help to provide confinement to the relativistic gas.

Jets powered by the rotation of a black hole (Blandford-Znajek mechanism) would presumably consist of a pure electron-positron pair plasma, while outflows from rotating discs are regarded as consisting of normal hadronic plus leptonic matter. However, since isolated black holes cannot sustain a magnetic field, a field threading the hole requires an accretion disc to keep it in place. If the accretion disc is cool, the conditions for outflow are sensitive to the field strength and inclination near the disc surface. But this dependence is attenuated in an ion-supported flow [45], where the temperature of the hadronic matter is near the virial temperature and the flow only weakly bonds in the gravitational potential of the accreting object. This may, in part, be the reason why powerful jets tend to be associated with the hard states in X-ray binaries for which the ion-supported flow (also called ADAF) is a likely model [46]. Therefore, it is quite probable that a jet accelerated by the hole is also supplied with ions besides electrons from the disc, rather than with a pure lepton pair plasma generated after quantum fluctuations and gamma-ray annihilation.

This possibility also suggests that the magnetic flux passing through a disc is a global quantity of the system rather than a function of local conditions near the center. Namely, the flux depends on the way it is transported through the disc as a whole. In fact, some similarities in the features and time variability of spectral states of very different brightness (c.f. VHS and LHS) [47, 48, 49], support the idea that the phenomenology of XRBs is not simply a function of the instantaneous accretion rate alone. A useful second parameter would therefore be a global quantity, a property of the disc as a body, which can vary among discs or with time in a given disc. As argued in [50], a promising candidate is the net flux of magnetic field lines crossing the disc since its value is determined only by inheritance from the initial conditions and the boundary conditions at its outer edge. In addition, it cannot be changed by local processes within the disc. An interesting observational connection is that the presence or quenching of jets could be related to variations in the global magnetic flux of the disc [50]. If the hard X-ray state is indeed one with a high magnetic flux in the inner disc, its connection with jets would be natural since the current theory strongly suggests that outflows are magnetically driven phenomena.

Although axisymmetry has been the standard working hypothesis, the energy carried in the form of the wound-up magnetic field can decay by internal dissipation in ways that do not occur in axisymmetric systems. Indeed, a way of dissipating magnetic energy is to generate the flow from a non-axisymmetric rotating magnetic field. A classic example of such a flow is the pulsar wind generated by a rotating neutron star with a magnetic field inclined with respect to the rotation axis. Thus a non-axisymmetric rotating magnetic field turns out to be a very efficient way of accelerating the flow to high Lorentz factors [51, 52].

At short length scales, dissipation of magnetic energy by reconnection of field lines can be very efficient and have striking effects on the flow. For example, the conversion of

Poynting flux into kinetic energy by wasting magnetic energy. This mechanism does not require an increasing opening angle of the flow lines. If the dissipation is a consequence of magnetic instabilities, it works much better at high degrees of collimation. If it is due to reconnection in an intrinsically non-axisymmetric flow, it works independently of the degree of collimation [51]. The mechanism is also effective at distances significantly beyond the Alfvén radius.

## **Jet's scale sectors and particle interactions**

The energy release powering a relativistic outflow takes place near the black hole, at a distance of the order of  $50R_g$  (about  $10^7$  cm in the case of a microquasar). On the other hand, narrow jets seen at radio wavelengths may appear on scales up to ten orders of magnitude above that. The collimation of the flow, however, may take place on intermediate scales, large compared with the Alfvén radius, at least for very narrow jets. Such intermediate length scales can also be crucial for acceleration to high Lorentz factors, although the region around the Alfvén radius plays the main role in standard axisymmetric centrifugal acceleration processes.

Once the jet is launched, it may interact with other material coming from the accretion disc or the stellar companion. For instance, an accretion disc wind can enhance collimation and stability but a strong stellar wind may lead to jet bending and even disruption into separate jet clumps.

In any case, interaction with the environment may induce shock formation and its radiative counterpart may be observable either as a transient phenomenon, when the outflow penetrates for the first time through the surrounding medium, or as a steady one when the jet feeding is continuous, thus allowing re-collimation shocks.

Although the jet's environments at large scales may be quite different among microquasars, depending on the local ISM of the galaxy and the strength of the companion's wind, jets must terminate abruptly or be softly diffused away. In the first case it is expected that they get stopped against the ISM by disruption or via shocks, inducing different radiative outcomes. A classical example of the interaction between a XRB jet and its environment is the case of SNR W50, where the jets of the microquasar SS 433 have strongly deformed the remnants up to the degree scale (e.g. [53]).

In order to describe the jet, we can divide it into four scale regions as explained in [54]. The jet base region, close to the compact object ( $50 - 1000R_g$ ), the binary system scale region (typically  $10^{10} - 10^{13}$  cm in XRBs), a third one at middle scales (around  $10^{15} - 10^{16}$  cm), and the termination region of the jet, where it ends interacting somehow with the interstellar medium ( $\geq 10^{17}$  cm for XRBs).

Actually, at the base the jet could be further subdivided in two parts: a close, magnetically dominated sector, where particle acceleration may happen by magnetic energy dissipation via magneto-hydrodynamical (MHD) instabilities (as it happens in extragalactic jets [55]), and a shock sector where the magnetic field is in subequipartition and acceleration likely occurs via Fermi processes. A magneto-centrifugal mechanism also operates very close to the rotating object (see e.g. [56, 57]). If jet velocities are high enough at the base, the dense available photon and matter fields from accretion disc and corona could



allow the converter mechanism to take place (see e.g. [58, 59]). Magnetic field reconnection in the surrounding corona can also inject a nonthermal population of particles into the jet enriching the internal dynamics (see e.g. [60] and references therein).

As we have already seen, we can assume that the presence of both leptonic and hadronic matter in the jet is a natural consequence of its accretion origin. The relevant radiative mechanisms at the base are leptonic synchrotron emission (see e.g. [61]), relativistic Bremsstrahlung from electrons interacting with jet ions, synchrotron self-Compton (SSC) (see e.g. [62]) and inverse Compton scattering with corona and disc photons (see e.g. [63, 64]), all of which depend on the dominant local energy balance. Regarding hadronic processes, there are several mechanisms that could produce high energy radiation in the form of gamma rays and neutrinos, and as a by-product, low-energy emission from secondary particles. Two of these mechanisms are collisions of relativistic jet protons against cold ions (p-p scattering), and with photons (photo-meson production). Ions and multi-wavelength photons can have any origin, from the accretion disc or the external medium. Relativistic proton collisions with ions and photons produce neutral pions that decay into gamma rays as well as charged pions that decay into muons and neutrinos (going in turn into electrons and other neutrinos). Another possible hadronic mechanism is photo-disintegration, which requires the presence of ultra high energy heavy nuclei and a dense field of target photons of large-enough energy. This process produces lower-mass hadrons and gamma rays.

In the second jet sector, at binary system scales, plausible mechanisms for generating relativistic particles in the jet are the Fermi processes: shock diffusive (Fermi I), random scattering (Fermi II), and shear acceleration (see e.g. [65]). The Fermi I mechanism could take place due to internal shocks in the jet; Fermi II acceleration could take place if magnetic turbulence is strong enough, with high Alfvén velocity; shear layers would be a natural outcome in laterally expanding jets or any time different jet vs. medium velocities take place. Interactions with the stellar wind may also trigger particle acceleration through a recollimation shock formed in the jet that expands against the dense material expelled by the companion star (see e.g. [66]). The velocities of the different shocks could be either mildly or strongly relativistic. In the latter case, the converter mechanism may be effective in very bright star systems. At such binary system scales, possible radiative leptonic processes are synchrotron emission (see e.g. [67]), relativistic Bremsstrahlung (see e.g. [68]), SSC (see e.g. [69, 70]), and external IC (see e.g. [70, 71, 72, 73]). However, jet proton collisions with target nuclei of the stellar wind (see e.g. [74]) seem to be the most efficient hadronic process at these scales. As we shall further discuss, this mechanism would lead as well to neutrino production (see e.g. [75, 5]). Other hadronic processes expected in this sector are photomeson production (see e.g. [76]) and photodisintegration (see e.g. [77]).

At middle scales, intermittent ejections at larger time scales (hours to days) could create shocks [54]. Additionally, Fermi-II type and shear acceleration could drive a continuous outflow at these scales (c.f. intra-knot regions of extragalactic jets; e.g. [78]). Given the high jet/medium relative ram pressure at these scales, the environment influence is not expected to be significant. Here, the emission is usually characterized by synchrotron radiation; stellar IC upscattering is quite inefficient because of the large distances to the companion star rarify star photons. Nevertheless, for powerful ejections, SSC could still be significant (see e.g. [69]). Regarding the particle energy distribution,

its evolution is likely dominated by convective and adiabatic energy losses [79].

At the jet termination region, the inertia of the interstellar external medium plays an important dynamical role (c.f. AGN hot spots and radio lobes, e.g. [80]). When the outflow hits the interface with the external plasma, two shocks may be formed; one moving backward into the jet and another moving forward (the bow shock). Fermi-I type acceleration mechanism then seems to be plausible, although high diffusive and convective rates in the downstream regions of both the forward and reverse shocks could prevent efficient acceleration. It is also possible that MHD instabilities mix the jet matter with the interstellar medium without forming strong shocks (see e.g. [81]). If, on the other hand, particle acceleration and confinement were efficient, then synchrotron, relativistic Bremsstrahlung, and IC radiation could be produced there and eventually detected from nearby sources (see e.g. [82]). Hadronic acceleration could take place as well, which could lead to lower energy production and secondary leptonic emission.

## Jets from neutron stars

Some particular features make it worth addressing separately the issue of neutron stars in the context of XRBs. Recently, the Spitzer Space Telescope opened a new observational window for the study of jets in low-luminosity neutron star X-ray binaries. Observations of the NS ultracompact XRB 4U 0614+091 revealed the first results from the follow-up multi-wavelength observations in the radio band (VLA), mid-IR/IR (Spitzer/MIPS and IRAC), near-IR (SMARTS), optical-UV (Swift/UVOT), soft and hard X-rays (Swift/XRT and RXTE), the best coverage of a NS XRB to date [83].

With the present data, sometimes it is possible to perform an estimate of both the total jet power and the fraction of the accreted power channeled into the jet. Moreover, observations have generally shown evidence for an association between the formation of a jet and an X-ray state transition (c.f. the NS XRB GX 17+2).

XRBs holding a neutron star show some common features with BH XRBs. Remarkably, the presence of steady jets in the low state (below a few percent of  $L_{\text{Edd}}$ ) show a correlation between  $L_X$  and  $L_R$ . On the other hand, the occurrence of transient outflows at high luminosities (near  $L_{\text{Edd}}$ ), and even rapid X-ray state changes have also been observed. All this indicate a coupling between the jet and the inner accretion disc which does not depend on the nature of the compact object. Nevertheless, besides the similarities, some differences deserve attention. Particularly, the steeper relation between radio and X-ray luminosities,  $L_R \propto L_X^{1.4}$ , signaling that neutron stars remain less radio-loud than BH for a given X-ray power.

In order to compare NS and BH samples, it is important to know the common value of  $L_X$  at which it should be done. As argued in [84], the correlation between radio luminosity and jet power  $L_J$  should be compared at the least radiatively inefficient point, while still in the hard state, therefore producing a steady jet in both samples. This point corresponds to the brightest LHS / LAS (low hard atoll states). Comparison of the fits to the NS and BH samples indicates that at  $L_X \sim 0.02L_{\text{Edd}}$ , the ratio of radio luminosities is  $\sim 30$ . As noted in [85], assuming a scaling  $L_R \propto L_J^{1.4}$  this indicates that neutron star jets are about one order of magnitude less powerful than black hole jets at this X-ray

luminosity. This implies that  $L_J \propto L_X^{0.5}$  for BHs and  $L_J \propto L_X$  for NS [84]. In the first case, it is indicative of a radiatively inefficient accretion, in the sense that most of the liberated gravitational potential is carried kinetically in the bulk flow and not radiated.

Assuming that the relation between  $L_J$  and the mass accretion rate of the CO,  $\dot{m}$ , is the same for BH and NS XRBs, Migliari and Fender show that  $L_X \sim \dot{m}$  for NS and  $L_X \sim \dot{m}^2$  for BHs. The different coupling between  $L_X$  and  $\dot{m}$  ensures that the systems remain fixed in a state as the accretion rate changes. Thus the difference between  $L_R/L_X$  correlations is that NS are in a X-ray dominated state and BHs are in a jet dominated state.

It is generally accepted that very high magnetic fields at the surface of the NS inhibit the production of -steady- jets while a large amount of energy can be extracted from magnetic fields to power extremely energetic -transient- outflows. Although it is not clear the role of the magnetic field at the surface of a NS in the production of jets, it is believed that the higher the magnetic field is the lower the jet power should be.

Magnetic fields produced in NS extend from above  $10^{12}$ G, in classical X-ray pulsars, where jets are excluded at any accretion rate <sup>3</sup> [87, 84], down to  $10^{7-8}$ G in other sources connected to XRBs with jets such as atoll and Z-type systems [86]. In the presence of jets, the interval of accretion rates also covers a wide range, from less than 0.1% of the Eddington rate for millisecond X-ray pulsars, up to the Eddington critical rate for Z-sources.

The conditions for an XRB to undergo a microquasar phase, i.e. the generation of jets, are given by a relationship between the magnetic pressure  $P_B = B^2/8\pi$  and the hydrodynamic pressure  $P_p = \rho v^2$ , where  $\rho$  is the matter density and  $v$  its velocity. First, the magnetic field at the surface has to be relatively weak. Second, the magnetic field lines have to be already twisted close to the CO [88]. The appropriate regime for jet launching has thus been determined by studying the quotient between the CO radius and its Alfvén radius  $R_A$  (the distance where  $P_B = P_p$ ). The basic condition for jet formation is  $R_A/R_* = 1$  ( $R_A/R_{LSO} = 1$ ),  $R_*$  being the neutron star radius and  $R_{LSO}$  the last stable orbit of the BH. This condition implies that the accretion disc arrives down to the surface of the CO, and hence guarantees that  $P_B < P_p$  is valid in the whole disc. It allows quantifying the upper limit of the magnetic field strength as a function of the mass accretion rate [86]. As a result of this analysis, for a Kerr BH accreting at the Eddington rate, the magnetic field cannot exceed  $5 \times 10^8$ G, while in the case of Z-sources at the same rate, a magnetic field below  $B = 10^{8.2}$  G should be in order to make possible the generation of jets. This upper limit fits the observational estimative of [89] for Scorpius X-1. Atoll-sources, on the other hand, are potential sources for generating jets provided  $B \leq 10^{7.7}$  G. Evidence of jets in these kind of sources has been already found in [90, 91].

---

<sup>3</sup> Different from millisecond X-ray pulsars where it is not excluded that could develop jets, at least for sources with  $B \leq 10^{7.5}$ G [86]. In this case the source could switch to a microquasar phase during maximum accretion rate. The millisecond source SAX J1808.4-3658 shows indeed hints of a radio jet [84].

## VHE gamma-rays emitters

Some of the VHE gamma-ray sources detected in the last few years [92, 93, 94, 95, 96] have been identified with previously known X-ray binary systems [97]. Recently, Cygnus X-3, another well-known microquasar, has been also associated with a steady high energy gamma-ray source [98]. These detections, together with previous low energy observations, demonstrate the diversity of MHD processes underlying manifestly correlated non-thermal emission from XRBs with relativistic outflows.

As we have already mentioned, in a microquasar scenario VHE gamma-rays are supposed to be produced in the intersection zone common to intra-jet relativistic particles and external thermal matter plus radiation fields (e.g. [1]), and even fully within the jet's bulk [6]. The variability of the emerging signals and the spectral properties of the sources depend on several conditions and parameters. To estimate the TeV emission from these systems one has to take into account their intrinsic possibility of accelerating particles up to the TeV - PeV energy scale, the different radiative mechanisms, and the absorption of the produced VHE flux. In some cases, depending on the orbital phase and the intensity of companion and disc photon fields, the absorption can be strong enough for signals to lie below the sensitivity of current detectors [99].

Inverse Compton processes should produce significant VHE fluxes when external photon fields penetrate into the jet and are scattered off by VHE leptons. Among IC boosting, there are contributions to IC from leptonic self-generated synchrotron photons and relativistic Bremsstrahlung that should enhance the total VHE leptonic output. On the other hand, when  $\rho_m > \rho_k$ , strong synchrotron losses can attenuate this channel and reduce gamma-ray production. Intense VHE gamma-ray fluxes are generated through the decay of neutral pions from photomeson reactions and from pion production in relativistic collisions of protons in the jet against cold ions from the wind or the jet itself.

As explained in [6], the gamma-ray luminosity also depends on the fraction  $q_{\text{rel}}$  of the kinetic luminosity  $L_k$  transferred to the accelerated (relativistic) plasma. There, the authors have estimated the gamma-ray production in the heavy jets of SS 433 out of relativistic hadronic processes. By using the HEGRA upper limit on the VHE flux from this source, the value of  $q_{\text{rel}}$  for accelerated ultra-relativistic protons is maximally constrained by  $q_{\text{rel}} < 3 \times 10^{-4}$  (considering that HEGRA observations took place during unknown precessional phases). The last MAGIC observations, performed during the lowest absorption phases allow a more stringent constraint for the hadronic fraction ( $q_{\text{rel}} < 7.4 \cdot 10^{-5}$ ) [100] which, given the expected sensitivity of Icecube, is still above the lowest testable limit of our model [6].

## *VHE Flares*

Besides steady emission, short-lived ejections are frequent in microquasars. These are mostly seen in the transitions between the LHS to the HSS, although the flaring behavior is not limited to the state changes and is quite unpredictable (c.f. GRS 1915 +105 or Cyg X-3). The kinetic power released in such episodes can exceed  $10^{39}$  erg /s, with intense

radiation fluxes at all wavelengths. However, clear signals of VHE emission from GRS 1915 +105, Cyg X-1, Cyg X-3 and SS 433 remain undetected. In fact, apart from the steady TeV emission observed in the 4 galactic HMXBs, PSR B1259-63, LS I+61 303, LS 5039, Cyg X-1, clear evidence of a TeV flare has just been found in Cyg X-1. In the case of LS I+61 303, in addition to the periodic TeV emission, with a maximum at phase 0.6, it has been seen a flaring activity peaking around phase 0.8 [101]. Additionally, there is also a temporal coincidence between the TeV and the X-ray flare [102] as noted in [103]. LS 5039 presents also flaring TeV emission superposed to the periodic regular light-curve around phase 0.8.

The correlation between hard X-ray and TeV emission should provide more close constraints, since both signals could be produced by the same particle population or with a similar timescale [100]. However, the multifrequency correlation could be present only at some stages of the flare [95], rendering the start of TeV outburst detections a difficult task. The non-detection of any transient signal could be related to a high absorption in the inner regions of these systems. The gamma-ray attenuation due to stellar and accretion disc photon fields could in any case transfer the luminosity to lower gamma-ray energies through electromagnetic cascades [3, 104]. This would increase the fluxes at appropriate ranges for observatories like Fermi, providing information about the triggering of VHE gamma-ray and its relation with HE radiation in these systems [105]. It is worth noting also that the detection of outbursts at radio and IR wavelengths can be related to an increase of the activity also at VHE, although the delay between them could range from hours to days [69].

Regarding the variability of the emission, several factors are relevant. Injection can change due to variations in the accelerator, e.g. injection power and injection spectrum. Target densities could vary as a consequence of stochastic changes in the magnetic, photon, and matter fields. Geometry can evolve because of orbital motion or jet precession. Everything could affect anisotropic gamma-gamma absorption and scattering or photon boosting. Thus, the time scales of the variability can be linked to a lot of mechanisms including injection, radiative cooling, particle escape, and macroscopic motion.

So far, it has been experimentally established that the variability of gamma-ray sources is modulated with the orbital period although short-timescale flares are also observed [95, 106]. As mentioned, the presence of jets in some of the massive gamma-ray binaries implies that scattering of relativistic particles against the stellar wind of the primary seems unavoidable [74]. Since there are increasing reasons to think that the winds of hot stars have a clumped structure (e.g. [107, 108]) if the jet interacts with the stellar wind, the putative gamma-ray emission would present a variability related to the structure of the wind. Thus, the detection of rapid stochastic variability, quite distinct from long-term periodic variations, as orbital and precessional, could be used to understand the structure of the wind itself [109].

Notwithstanding, intrinsic disturbances in the jet (see e.g. [110, 111]) can also produce an aperiodic variability that might be confused with jet/clump interactions. Fortunately, as signaled in [109], intrinsic variability in the jet would likely be preceded by a change in the accretion disc X-ray activity, whereas in the case of a jet/clump interaction, the effect should be the opposite; first, the gamma-ray flare would appear, and then, a nonthermal X-ray flare produced by the secondary electrons and positrons (as well as the primary electrons injected into the clump) would show up. Depending on the magnetic

field and the clump density, the X-ray radiation could be dominated by synchrotron, inverse-Compton, or Bremsstrahlung emission, with a total luminosity related to that of the gamma-ray flare. Simultaneous X-ray observations with gamma-ray observations could be useful to distinguish jet/clump events from intrinsic variability produced by the propagation of shocks in the jets.

## Neutrinos

In general, arguments supporting predictions of discrete neutrino sources are based on the so-called  $\gamma$ - $\nu$  connection [112]. Photohadronic processes and proton scattering off nuclei are the most important astrophysical neutrino production mechanisms and they also produce gamma-rays. By identifying the brightest steady gamma-ray sources, we identify the most likely neutrino point sources to be surveyed. Of course, a source can be gamma-ray intense without being neutrino significant if the gamma-rays originate from leptonic processes. Conversely, a bright neutrino source can be gamma-ray dim if photon production is attenuated at the origin or along its path. At EGRET and GLAST energies ( $E \sim 100$  MeV - 10 GeV), attenuation by the extragalactic background is unimportant, even for the highest redshift objects. Thus, the EGRET catalog should be exhausted to identify the brightest gamma-ray sources and, by the above argument, the most probable neutrino point sources. The new discoveries with HESS, MAGIC, and VERITAS at gamma-ray TeV energies are especially significant for understanding and searching other galactic neutrino sources.

High-energy neutrino production takes place in a hadronic scenario and results from proton-ion interactions and photohadronic processes. The dominant channel for neutrino production involves the production of pions coming from these reactions. On average, neutron plus charged-pion reactions take place one third of the time while proton plus neutral-pion production occurs on two thirds. The outcome is therefore one high-energy lepton and three high-energy neutrinos for every four high-energy gamma rays (neutron decay produces a neutrino but just  $\sim 1\%$  energetic, in favor of the resulting proton momentum [112]). Since neutrinos carry only 1/4 of the energy radiated in electromagnetic secondaries, any high-energy neutrino source should be a strong gamma-ray source, were it not for gamma-ray opacity which can seriously modify this expectation [99].

For such gamma-ray sources, the selected neutrino sources should be those which IceCube could discriminate above the cosmic-ray neutrino induced background. At  $E \geq 1$  TeV, this background is at  $n_\nu \geq 0.4$  neutrinos/yr per square degree, and twice this value for  $E \geq 10$  TeV [113]. To be detected with a km-scale facility, the neutrino flux, and therefore the photon flux, must be above  $10^{-4}$  ergs/cm<sup>2</sup> [114].

In the Third EGRET catalog [97], several TeV gamma-ray sources that fit this criterion can be found, particularly 3EG J1824-1514 [115] and 3EG J0241+6103, respectively associated with the HMXBs LS 5039 [92] and LSI +61 303 [94]. Models for these gamma-ray emitters as potential neutrino sources have been developed in [5, 116, 33, 117] and their microquasar nature inspired also neutrino predictions in systems like SS 433 [6] though not found yet in the TeV range, probably due to intense local opacity [99].

Present and upcoming experiments like ICECUBE (e.g. [118]), ANTARES (e.g. [119]) and NEMO (e.g. [120]) are expected to show exciting new horizons in neutrino astronomy.

## MODEL FOR HIGH ENERGY EMISSION IN XRBS WITH JETS

In order to make a model approach to high energy emission in binary systems with jets, some geometrical assumptions are in order. Following [121] we can assume that jets are well collimated and conical-shaped, with small half-opening angles ( $\xi \leq 5^\circ$ ). The jet radius thus reads  $r(z) = z \tan \xi$  and its structure is completely defined all along. It is also reasonable to assume the jet injection point at a distance  $z_I = 50R_g$  where  $R_g = GM_C/c^2$  is the gravitational radius of the ejecting object (typically  $\simeq 10^{7-8}$  cm from a stellar CO).

The jet power and the accretion rate are related by  $\dot{M}_j = \frac{1}{2} q_j \dot{m}$ , assuming  $\dot{m} = q_a L_{\text{Edd}}$  and  $q_j, q_a < 1$  (the 1/2 factor accounts for the existence of a counter-jet). The kinetic luminosity of the jet can be written as  $L_{Jk} = \dot{M}_j / E_b m_p$  where  $E_b$  is the bulk kinetic energy and  $m_p$  the jet particle mass. The jet kinetic energy density is  $\rho_k(z) = L_{Jk} / \pi r_j^2 v_b$ , (erg/cm<sup>3</sup>) where  $v_b$  is the velocity (the subindex <sub>b</sub> is for bulk quantities). Following with the jet-accretion coupling hypothesis, we assume that a considerable part of the Eddington luminosity ( $\sim 10\%$ ) goes into the jet [122] so that  $L_{Jk}$  could attain up to  $\sim 10^{38}$  erg s<sup>-1</sup>. This power is carried among leptons and hadrons, a small fraction of which will be ultra-relativistically accelerated within the jet.

As we have seen, the jet can be divided in several sectors where particles are accelerated and cooled by different means. Following [65] the stochastic motion in a collimated outflow results in a mean electric field in the  $z$  direction. Defining the rate of energy variation by means of  $t^{-1} = E^{-1} dE/dt$ , the rate of stochastic electromagnetic acceleration of a  $eZ$ -charged particle up to an energy  $E$  is given by  $t_{\text{acc}}^{-1} \approx \eta c eZ B/E_p$  (CGS), where  $\eta$  is the efficiency of the accelerator (e.g. [123]). In the energy equipartition region, where the magnetic energy density  $\rho_m$  equals the kinetic density  $\rho_k$ , the magnetic field reads  $B(z_E) = \sqrt{8\pi\rho_k(z_E)} = 2\sqrt{\dot{M}_j v_b / z_E \tan \xi}$  and reaches very high values. It varies with distance as  $(z_E/z)^m$ ,  $1 \leq m \leq 2$  [124]. Here we assume that just above the jet injection point,  $z_I$ , the jet is magnetically dominated while in the acceleration/transport zone,  $z_0 \leq z \leq \sim 5z_0$  ( $z_0 \sim 10z_I$ ), the magnetic field is weaker and the jet is dynamically dominated,  $\rho_k > \rho_m$  (see [125]). In this zone we have to consider a transport equation in order to take into account energy losses as well.

Assuming shock diffusive acceleration near the base, the injection rate is a canonical second-order power-law in the particle energy. On the other hand, conservation of the number of particles demands that the current evolves with  $z^2$ . Hence,  $J'(E', z') = cK_0/4\pi E'^{-2} (z_0/z)^2$  [126], where primed quantities are in the jet frame. In the absence of sinks or sources, other than the termination and injection points, the injection function of particles,  $Q(E, z)$ , must satisfy a continuity relation with the current [127]. After some

relativistic considerations, for this function we obtain

$$Q(E, z) = R_0 \left( \frac{z_0}{z} \right)^3 \frac{\Gamma_b^{-2} \left( E - \beta_b \sqrt{E^2 - m^2 c^4} \cos i_j \right)^{-2}}{\sqrt{\sin^2 i_j + \Gamma_b^2 \left( \cos i_j - \frac{\beta_b E}{\sqrt{E^2 - m^2 c^4}} \right)^2}} \quad (1)$$

in an observer's reference frame making an angle  $i_j$  with the line of sight<sup>4</sup>. The normalization constant  $R_0$  is the power density at the acceleration/injection point  $z_0$  and results by specifying the relativistic lepton (proton) luminosity of the jet

$$L_{e,p} = \int_V d^3 r d\Omega \int_{E_{e,p}^{(\min)}}^{E_{e,p}^{(\max)}} dE_{e,p} E_{e,p} Q_{e,p}(E_{e,p}, z), \quad (2)$$

where  $E_e^{(\min)} = 1$  MeV,  $E_p^{(\min)} = 1.2$  GeV, and the maximum energies will be obtained by equating the acceleration rate to the energy loss rate. The fraction of the total kinetic power carried by the ultra-relativistic primary particles in the jet is parameterized by means of  $q_{\text{rel}}$ , namely  $q_{\text{rel}} L_k = L_{\text{rel}} = L_p + L_e$ . We can further assume a simple relation between the proton and electron luminosities as given by an hadronicity parameter,  $h$ , such that  $L_p = h L_e$  [128].

### Energy losses

The main particle processes responsible for the energy cooling in a leptonic/hadronic jet are the following.

*Synchrotron cooling:*  $e^\mp + (B) \rightarrow e^\mp + \gamma'$

Of course, fast moving charged particles emit strong synchrotron radiation<sup>5</sup>. Its rate is given by  $t_{\text{sync}}^{-1} = \frac{4}{3} \left( \frac{m_e}{m} \right)^3 \sigma_T B^2 \gamma / m_e c$  8 $\pi$  (e.g., [123]), where  $m$  is the mass of the particle and  $E = \gamma m c^2$  its relativistic energy.

The power per unit energy of the synchrotron photons radiated by  $N_{e,p}(E, z)$  charged particles is  $\epsilon_{\text{syn}}^{(e,p)}(E_\gamma) = \int d\Omega \alpha \int_{E_{e,p}^{(\min)}}^{E_{e,p}^{(\max)}} dE_{e,p} P_{\text{syn}} N_{e,p}(E, z)$ , where  $P_{\text{syn}}(E_\gamma, E, z, \alpha)$  is the power radiated by a single particle of energy  $E$  and pitch angle  $\alpha$  (e.g. [129]) and

---

<sup>4</sup> Note that the angle  $i_j$ , as well as  $Q$ , can depend on time. In the first case this is easy to handle since it is a function of precession; in the second it depends on several factors, including instabilities and stochastic processes.

<sup>5</sup> Synchrotron radiation is an analog to bremsstrahlung, differing in that the force which accelerates the electron is a macroscopic or large scale magnetic field. Bremsstrahlung is the electromagnetic radiation produced by a sudden slow down or deflection of charged particles, especially electrons, passing through matter in the vicinity of the strong electric fields of atomic nuclei or ions. In a broad sense, bremsstrahlung is the radiation emitted when any charged particle is accelerated by any force, but to a great extent, is a source of photons in the ultraviolet and soft x-ray region for the investigation of atomic structure.



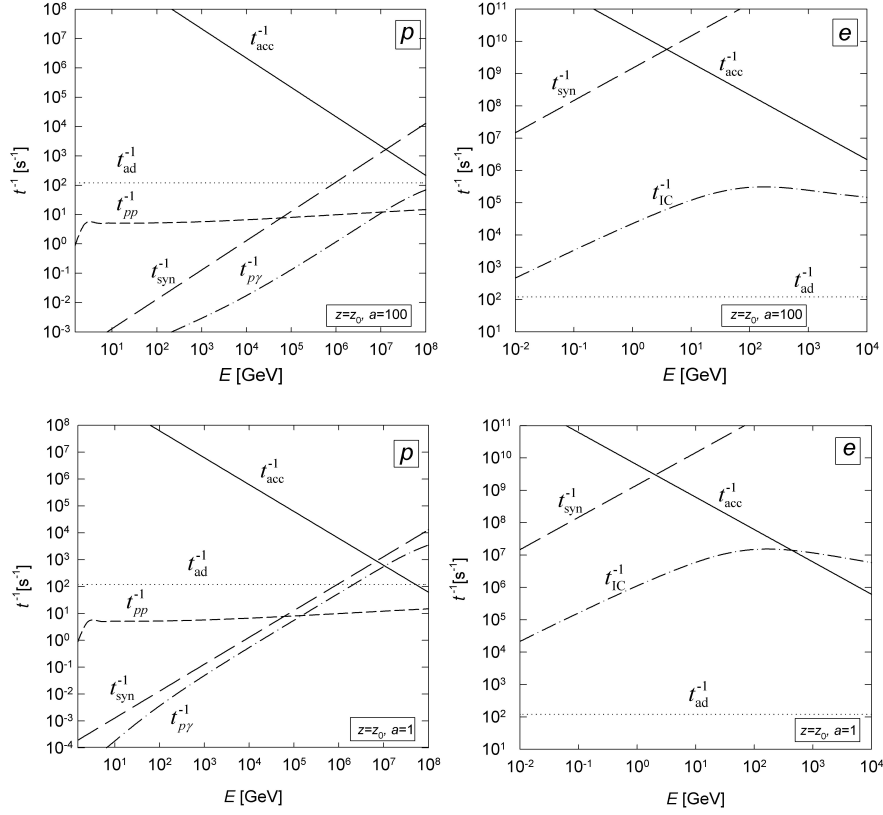


**FIGURE 3.** Accelerating and cooling rates for protons (left) and electrons (right) at the base of a hadro-leptonic jet dominated by protons ( $h = 100$ , top) and with power equipartition ( $h = 1$ , bottom). Figures from [127] ( $a$  is the hadronicity  $h$  in the present notation).

the total luminosity can be obtained by integrating in the volume of the region of acceleration  $L_{\text{syn}}^{(e,p)}(E_\gamma) = \int_V d^3r E_\gamma \epsilon_{\text{syn}}^{(e,p)}$ .

*Inverse-Compton cooling:*  $e^\mp + \gamma \rightarrow e^\mp + \gamma'$

In turn, ambient photons serve as targets for the electrons themselves and the corresponding rate is given by  $t_{\text{IC}}^{-1}(E, z) = \frac{4}{3} \left(\frac{m_e}{m}\right)^3 \sigma_T \rho_{\text{ph}} \gamma / m_e c$ , where  $\rho_{\text{ph}} = \int d\epsilon \epsilon N_{\text{ph}}(\epsilon, z)$ , integrated in  $\epsilon < m_p^2 c^4 / E$ , is the photon energy density [123]. In the case of self-synchrotron Compton scattering, the radiation density can be approximated by  $N_{\text{ph}}(\epsilon, z) \approx n_{\text{synchr}}(\epsilon, z) = \frac{\epsilon_{\text{syn}}}{\epsilon} \frac{r_j(z)}{c}$ , as in [126].

The IC spectral luminosity reads

$$L_{\text{IC}}(E_\gamma) = E_\gamma^2 \int_V d^3r \int_{E_{\text{min}}}^{E_e^{\text{max}}(z)} dE_e N_{e,p} \int_{\epsilon_{\text{min}}}^{\epsilon_{\text{max}}} d\epsilon P_{\text{IC}},$$

where  $P_{\text{IC}}(E_\gamma, E, \epsilon, z)$  is the spectrum of photons scattered by a charged particle of energy  $E$  [129].

Regarding protons, synchrotron and pure IC loss rates are more than 9 orders of magnitude less significant than for electrons, and the principal energy cooling mechanisms are the following.

$$\begin{aligned} \text{Photopion production: } p + \gamma &\rightarrow p + a\pi^0 + b(\pi^+ + \pi^-) \\ p + \gamma &\rightarrow n + \pi^+ + a'\pi^0 + b'(\pi^+ + \pi^-), \end{aligned}$$

where  $a, b, a', b'$  are the pion multiplicities of each channel <sup>6</sup>.

The photopion cooling rate is given by

$$t_{p\gamma}^{-1}(E, z) = \frac{c}{2\gamma_p} \int_{\frac{\varepsilon_{\text{th}}}{2\gamma_p}}^{\infty} d\varepsilon \frac{N_{\text{ph}}(\varepsilon, z)}{E_{\text{ph}}^2} \int_{\varepsilon_{\text{th}}}^{2\varepsilon\gamma_p} d\varepsilon' \sigma_{p\gamma}^{(\pi)}(\varepsilon') K_{p\gamma}^{(\pi)}(\varepsilon') \varepsilon'$$

where,  $\varepsilon_{\text{th}} = 145 \text{ MeV}$  [123]. Approximated expressions for the cross section  $\sigma_{p\gamma}^{(\pi)}$  and inelasticity can be found in [130]. Photopion production is the predominant  $p\gamma$  channel. It mainly occurs when protons collide with X-ray photons from the corona ( $2\text{keV} < E < 100\text{keV}$ ), for which, based on [131], we can adopt a Bremsstrahlung X-ray distribution  $n_X(E) = L_X e^{-E/(kT_e)} / 4\pi z_j^2 E^2 (\text{erg}^{-1}\text{cm}^{-3})$ , where  $kT_e \approx 30\text{keV}$  and  $L_X = 10^{36}\text{erg/s}$ .

*Photopair production:*  $p + \gamma \rightarrow p + e^- + e^+$ , is calculated using the same  $t_{p\gamma}^{-1}$  expression, but the soft photon density includes also the contribution of UV emission (particularly if there is an extended disc, as in SS433),  $n_{\text{ph}}(E) = 2E^2(hc)^{-3}(e^{E/kT_{\text{UV}}} - 1)^{-1}\pi R_{\text{out}}^2/z^2 + n_X(E)$ , with  $T_{\text{UV}} = 21000 \text{ K}$ , based on [132]. For this process we consider the expressions for cross section  $\sigma_{p\gamma}^{(e)}$  and inelasticity  $K_{p\gamma}^{(e)}$  given in [123]. See also [133] for a detailed discussion.

$$\begin{aligned} \text{Proton-proton cooling: } p + p &\rightarrow p + p + A\pi^0 + B(\pi^+ + \pi^-) \\ p + p &\rightarrow p + n + \pi^+ + A'\pi^0 + B'(\pi^+ + \pi^-), \\ p + p &\rightarrow n + n + 2\pi^+ + A''\pi^0 + B''(\pi^+ + \pi^-), \end{aligned}$$

where  $A, B, A', B', A'', B''$  are the pion multiplicities of each channel. Pure hadron collisions are crucial, particularly for VHE production. Now, the rate of  $pp$  collisions of ultra-relativistic protons against the cold ones is given by  $t_{pp}^{-1} = n(z) c \sigma_{pp}^{(\text{inel})}(E_p) K_{pp}$ , where the inelasticity is  $K_{pp} \approx 0.5$ , assuming that the projectile yields half of its energy for secondaries. The density of cold target particles in the jet at a distance  $z \geq z_0$  from the compact object is  $n(z) = (1 - q_{\text{rel}})L_k / \Gamma_b m_p c^2 \pi r_j^2 v_b$  and the cross section  $\sigma_{pp}^{(\text{inel})}$  is given in [134].

Finally, since the jet is laterally expanding with velocity  $v_b \tan \xi$ , there is also an *adiabatic cooling* rate given by  $t_{\text{ad}}^{-1}(z) = \frac{2}{3} v_b / z$  [68].

---

<sup>6</sup> At lower energies, one could also consider direct IC photon boosting by protons  $p + \gamma \rightarrow p' + \gamma'$  (see [130]) but it is irrelevant at high energies even in extreme radiation fields.

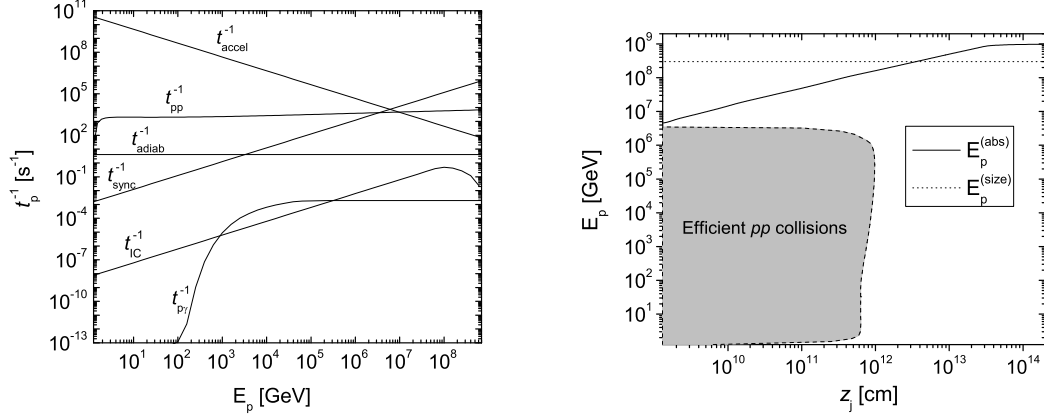


**FIGURE 4.** (Left) Proton accelerating and cooling rates. (Right)  $E$ - $z$  region where  $pp$  collisions are dominant. Note maximal proton energy values  $E_p^{\text{abs}}$  obtained from  $t_{\text{acc}}^{-1} = \sum t_{\text{loss}}^{-1}$ . Details in [6].

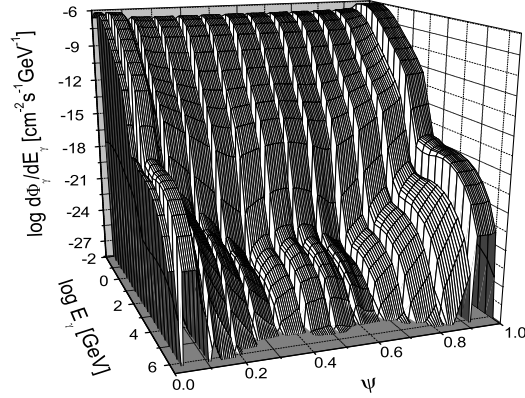


**FIGURE 5.** Differential gamma-ray flux from microquasar SS 433 arriving at Earth as a function of precessional phase and energy. In this case, (strong) absorption effects have been included. See details and discussion in Ref.[6].

The highest energies theoretically reached by the particles can be obtained from an equation  $t_{\text{acc}}^{-1}(E^{(\text{max})}) = \sum t_{\text{loss}}^{-1}(E^{(\text{max})})$  for each species of particle. Depending on the position  $z$  and the hadronicity  $h$ , one obtains different values of  $E^{(\text{max})}$  for leptons and for hadrons. See the results in Fig. 3 and Fig.4.

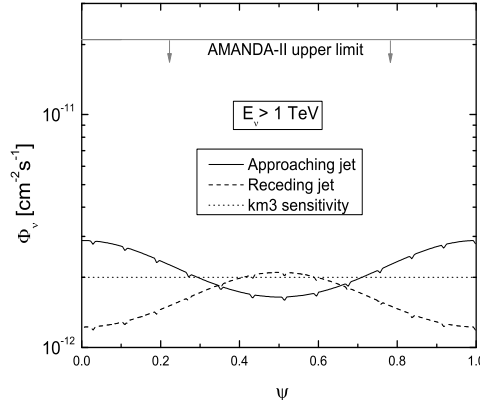


**FIGURE 6.** Neutrino flux ( $E_\nu > 1 \text{ TeV}$ ) arriving at Earth as a function of the jet precessional phase. The contributions of hadronic jet and counterjet are shown separately, solid line for the approaching jet and dashed line for the receding one (secondary losses neglected). The upper limit from AMANDA-II data and the expected  $\text{km}^3$  sensitivity are shown in grey solid line and dotted line respectively. Figure from [6]

### *The transport equation for primaries*

In each acceleration sector of the jet, and for each particle species, the steady state spectral primary particle distribution can be obtained as the solution of a transport equation

$$\frac{\partial [N_i(E, z) b_i(E, z)]}{\partial E} + \frac{N_i(E, z)}{T_i^{\text{esc}}(z)} = Q_i(E, z), \quad (3)$$

where  $b_i(E, z) \sim -E \sum t_{i \text{ loss}}^{-1}(E, z)$  and  $T_i^{\text{esc}}(z) \approx (z_i^{\text{max}} - z)/c$  is the escape rate from sector  $i$  ( $z_i^{\text{max}}$  is the termination point of this sector). The corresponding solution is

$$N_i(E, z) = \frac{1}{|b_i(E)|} \int_E^{E_i^{(\text{max})}} dE' Q_i(E', z) \times \exp \{ -\tau_i(E, E') / T_i^{\text{esc}} \}$$

with  $\tau_i(E, E') = \int_E^{E'} dE'' / |b_i(E'')|$  (e.g. [135]). The effect of particle acceleration is implicit in the (ultra-relativistic) injection function  $Q_i$  and the effect of deceleration is in the  $b_i$  function. As a matter of fact, a complete description of the evolution requires a time dependence of the functions, but a solution is still lacking. In each sector  $i$  of the jet and for each kind of particle the dominant acceleration mechanisms and cooling processes vary, as we have already explained. In order to simplify calculations though extracting enough dynamical features, we can assume a one zone acceleration approach and consider a small sector near the base  $z \gtrsim z_0$ , where shocks are more frequent. Taking into account a lower acceleration efficiency, a similar approximation can be exploited in the case of a clumpy wind (typically in HMXBs) colliding with the jet at middle scales (see [136]).

## Secondary particles and VHE luminosity

As we have mentioned above, the primary relativistic protons produce pions through inelastic interactions with matter and radiation. Charged pions in turn decay into muons and neutrinos, and muons then go into neutrinos and electrons:

$$\pi^- \rightarrow \mu^- \bar{\nu}_\mu \rightarrow e^- \nu_\mu \bar{\nu}_e \bar{\nu}_\mu, \quad \pi^+ \rightarrow \mu^+ \nu_\mu \rightarrow e^+ \bar{\nu}_\mu \nu_e \nu_\mu.$$

On the same footing, neutral pions decay into gamma-rays through the channel

$$\pi^0 \rightarrow \gamma\gamma.$$

The distribution of energetic gamma-rays results from the distribution of neutral pions. As a result of  $pp$  interactions, the gamma-ray emissivity, in units  $\text{GeV}^{-1}\text{s}^{-1}$ , reads

$$dN_\gamma(t, E_\gamma, z)/dE_\gamma = \int_{x_{\min}}^{x_{\max}} \sigma_{pp}^{\text{inel}}\left(\frac{E_\gamma}{x}\right) J_p\left(t, \frac{E_\gamma}{x}, z\right) F_\gamma\left(x, \frac{E_\gamma}{x}\right) dx$$

where the spectrum of produced gamma-rays  $F_\gamma(x, E_p)$  is given in [134], based on SIBYLL simulations of  $pp$  interactions including perturbative QCD effects;  $x$  is defined by  $E_\gamma = xE_p$ , for a primary proton with energy  $E_p$ , and the integration limits are chosen in order to cover the proton energy range where  $pp$  collisions dominate at each  $z$ . The spectral intensity of gamma-rays emitted from the jet can be obtained from

$$I_\gamma(t, E_\gamma) = \int_{z_0}^{z_1} dz \pi(z \tan \xi)^2 n_p dN_\gamma(t, E_\gamma, z)/dE_\gamma.$$

As for gamma-rays coming from photopion production at very high energies, the gamma-ray emissivity reads

$$dN_\gamma(t, E_\gamma, z)/dE_\gamma = \int N_p(E_p) n_{\text{ph}}(\varepsilon) \Phi(y, x) d\varepsilon dE_p/E_p.$$

Here, the distribution of the target photons of energy  $\varepsilon$  and the function  $\Phi$  can be found in [133] based on SOPHIA Montecarlo routines<sup>7</sup>;  $y = 4\varepsilon E_p/m_p^2 c^4 \geq 0.313$ .

Naturally, before decaying, secondaries are also free to interact (at a rate depending on the ambient density). Charged pions and leptons will be accelerated as described in the previous section, but they will also lose energy and emit radiation according to the processes discussed above. See contributions at different energies in Fig.7. On the other hand, the main channel for neutrino production is through charged pions into muons.

In the case of pions, one has  $b_\pi(E, z) = -E(t_{\text{syn}}^{-1} + t_{\pi p}^{-1} + t_{\pi\gamma}^{-1} + t_{\text{ad}}^{-1})$ . For the  $\pi p$  interactions  $t_{\pi p}^{-1}(E, z) \approx n(z) c \sigma_{\pi p}^{(\text{inel})}(E_p)/2$ , where  $\sigma_{\pi p}^{\text{inel}}(E) \approx (2/3)\sigma_{pp}^{\text{inel}}(E)$  based on the fact that the proton is composed by three valence quarks while the pion is formed by two

---

<sup>7</sup> As a matter of fact, one should also include kaon and  $\eta$  channels since they contribute noticeably in the production of secondaries's gamma-rays and leptons. These have accordingly been taken into account in the simulations [133].

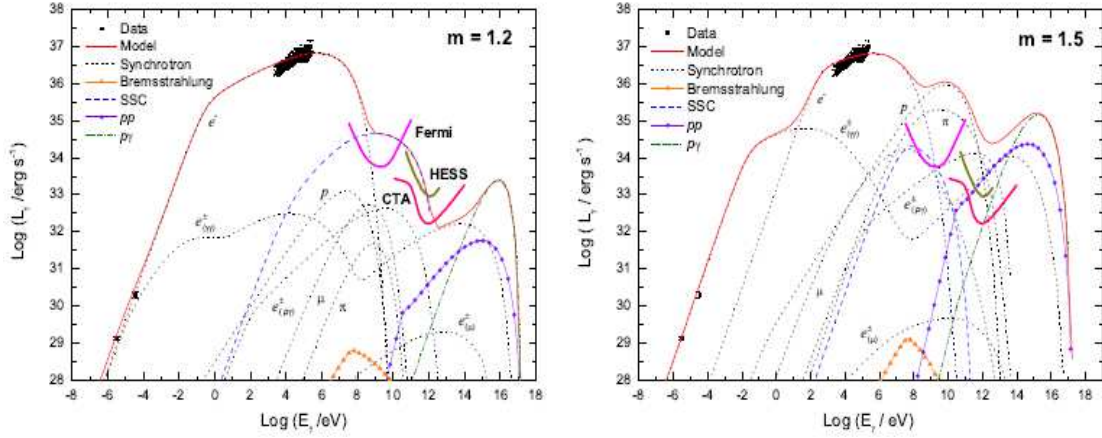


**FIGURE 7.** Best-fit spectral photon energy distributions for microquasar GX 339-4 ( $m$  is the magnetic field decay index). The subindexes ( $\gamma\gamma$ ), ( $p\gamma$ ) and ( $\mu$ ) indicate pairs created through photon-photon annihilation, photopair production and muon decay, respectively. The thick lines are the sensitivity limits of Fermi and HESS, and the predicted for CTA. Figures from [137].

[138]. As for the  $\pi\gamma$  interactions we estimate a cooling rate using the expression of  $t_{p\gamma}^{-1}$  properly adapted with the same argument (e.g. by replacing  $\sigma_{p\gamma}^{(\pi)} \rightarrow (2/3)\sigma_{p\gamma}^{(\pi)}$ ). Regarding muons,  $b_\mu(E, z) = -E(t_{\text{syn}}^{-1} + t_{\text{ad}}^{-1} + t_{\text{IC}}^{-1})$ , and we can ignore their interactions with primaries or pions. Since secondaries have short lifetimes, in the corresponding transport equations we have to consider  $t_{\text{esc}} = \min\{T_{\text{esc}}, T_{\text{dec}}\}$  with  $T_{\text{dec}}^{-1} = [2.6 \times 10^{-8} \gamma_\pi]^{-1} (\text{s}^{-1})$  for pions and  $T_{\text{dec}}^{-1} = [2.2 \times 10^{-6} \gamma_\mu]^{-1} (\text{s}^{-1})$  for muons.

The injection function for pions produced either by  $pp$  or  $p\gamma$  interactions,  $Q_\pi^{(pp)}(E, z)$  and  $Q_\pi^{(p\gamma)}(E, z)$ , can be found in [134]. The corresponding pion distributions,  $N_\pi^{(pp)}(E, z)$  and  $N_\pi^{(p\gamma)}(E, z)$ , obey an independent transport equation with the obvious replacements. We can use these to compute the different emitting processes for each charged species, and also as a source for generating the injection distributions of descendant muons.

In the case of muons, since right-handed and left-handed species have different decay spectra,  $dn_{\pi^\pm \rightarrow \mu_L^\pm; \mu_R^\pm}(E_\mu, E_\pi)/dE_\mu$ , it is necessary to consider their production separately, as discussed in [139]. Each of the resulting injection functions are put in the corresponding transport equations and, after adding helicities, one obtains the final spectral distributions of muons of each charge,  $N_{\mu^\pm}$ , originated from charged pions of both channels.

The total emissivity is the sum of the contribution of direct pion decays plus that of muon decays  $dN_\nu(E, z)/dE_\nu = dN_\nu/dE_\nu^{\pi \rightarrow \nu} + dN_\nu/dE_\nu^{\mu \rightarrow \nu}$  (see [139]). The differential flux of neutrinos arriving at the Earth is  $d\Phi_\nu/dE = \frac{1}{4\pi d^2} I_\nu(E)$ , where  $d$  is the distance to the source and the neutrino intensity  $I_\nu(E) = \int_V d^3r dN_\nu(E, z)/dE_\nu$  ( $\text{GeV}^{-1} \text{s}^{-1}$ ) depends on  $h$  and the jet half-opening angle  $\xi$ .

This quantity, weighted by the squared energy, is shown in Fig. 8 for a source at  $d = 2$  kpc, different values of the jet opening angle, and different values of  $h$ . As a guide, we also include a typical upper limit as derived from AMANDA-II data, as well as the

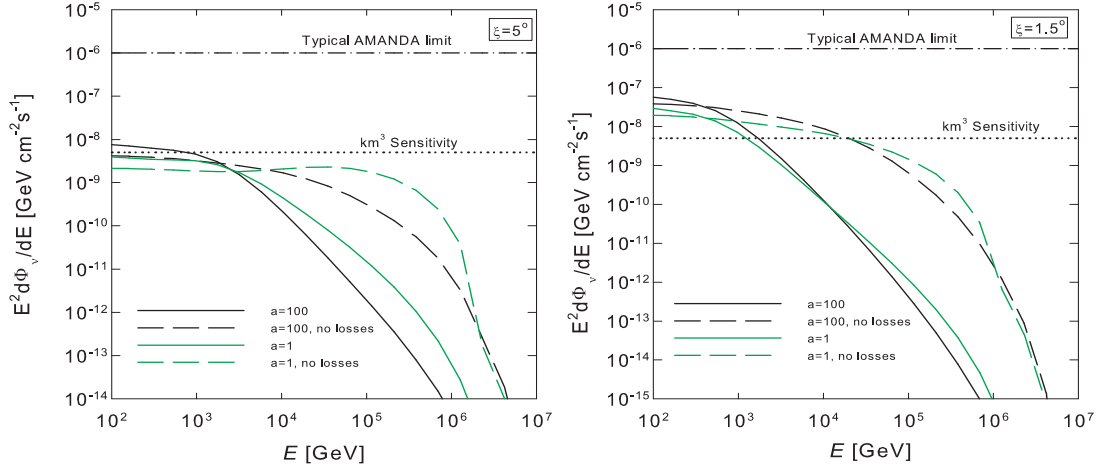


**FIGURE 8.** Differential neutrino fluxes (weighted by energy squared). Cases  $\xi = 5^\circ$ ,  $1.5^\circ$  are shown in the left and right panels respectively. Black lines correspond to  $h = 100$  and green lines to  $h = 1$ . Solid (dashed) lines: losses of secondary pions and muons considered (neglected). Figure from [127].

expected sensitivity for the next generation neutrino telescope ([140], see also [141]).

## Non-XRB VHE sources

In addition to X-ray stellar-mass binaries with a compact object, either galactic and extragalactic star-forming regions or active galactic nuclei and gamma-ray bursts are strong candidate sources for very high-energy emission.

### *Jets and outflows from young stellar objects*

So far we have been discussing outflows ejected from neutron stars and black holes, namely dead stars. However, star-forming regions (SFR) can also develop relativistic jets and gamma-rays can be produced through different processes along their evolution, from dark clouds to open clusters [142]. From the experimental point of view, the discovery of the extended source TeV J2032+4130 in Cygnus OB2 by HEGRA in 2002 [143] marks a cornerstone on this subject. Recently, two other such gamma-ray sources have been detected, namely, Westerlund 2 [144] and W43 [145] revealing that SFR are significant candidates for the new generation of gamma-ray Cherenkov telescopes.

The jets of a massive young stellar object (YSO) propagate through the molecular cloud where a protostar is embedded, either ending in the interior of the cloud or breaking out at its surface where strong shocks are expected to occur. Even if obscure at optical wavelengths, jets have been observed in radio, revealing their characteristic long scale features (e.g. [146]). In early stages of star formation, the integrated luminosity of many individual protostars in a massive dark cloud can reach values of  $10^{33}$  erg/s

at gamma-ray energies up to 100 MeV [147]. Actually, the simultaneous emission of several such YSOs, can illuminate the cloud in gamma-rays producing a detectable source for instruments like EGRET and AGILE, while higher resolution telescopes like LAT (GLAST-Fermi satellite) are expected to resolve even the individual sources.

When massive stars are already formed, the collective effect of many stellar winds is expected to result in particle acceleration up to relativistic energies (e.g. [148, 149]). The clean detection of non-thermal radio emission coming from the colliding wind region of binary systems like WR140, WR146, etc., indicates that electrons [147] and protons [150] are being efficiently accelerated up to relativistic energies. In Wolf-Rayet / OB systems, like WR140, luminosities can reach up to  $10^{34}$  erg/s at  $E > 100$  MeV [151]. Finally, supernova explosions of very massive stars in SFR open clusters can also trigger collective shocks where particles can be accelerated [e.g. [152]].

The spectral energy distribution can be calculated on the same footing as in the XRB systems, taking into account both leptonic and hadronic shock acceleration and cooling by scattering with matter and radiation. In this case one also considers bremsstrahlung cooling<sup>8</sup>.

### *Extragalactic VHE emitters*

Besides galactic SFRs, star-forming galaxies might be also considered energetic gamma-ray emitters and likely energetic neutrino point sources. In both cases cosmic rays would be accelerated by the above mentioned mechanisms in order to produce these high-energy emissions. So far, however, only one extragalactic galaxy (the Large Magellanic Cloud) was detected with EGRET, with a dim integral gamma-ray flux  $1.9(+/-0.4) \times 10^{-7}$  ph/cm<sup>2</sup> s ( $E > 100$  MeV) [153]. Thus, based on the  $\gamma$ - $\nu$  connection, it would demand several years to detect neutrinos from the LMC using IceCube (unless there was an anomalous hardening of the spectrum) [112]. Nevertheless, the superpositions of the neutrino emission from star-forming galaxies should grant a background as derived from the synchrotron radio luminosity associated with cosmic-ray acceleration [154]. Other likely neutrino sources are gamma-ray bursters and TeV blazars since their bright and hard gamma-ray spectra could plausibly have a hadronic origin.

The leading model for gamma-ray bursters involves a relativistic fireball jet, where the gamma rays are produced from Fermi-accelerated particles in optically thin shocks (for a review see, e.g., [155]). In the so-called collapsar model for long-duration gamma-ray bursts (GRBs), the core of a massive star collapses to a black hole or neutron star, driving a highly relativistic jet which breaks out of the star [156]. Within this framework, high-energy neutrinos from relativistic proton collisions have been studied (e.g. [157, 158]) predicting energies up to  $E_\nu > 10^5$  TeV from external shocks [159, 160]. In addition, internal shocks can occur while the relativistic jet is still in the star, with a neutrino precursor burst of  $E_\nu \geq 5$  TeV emitted from an imprisoned jet that is dark in gamma

---

<sup>8</sup> Thermal bremsstrahlung from an ionized hydrogen cloud (HII region) is often called free-free emission because it is produced by free electrons scattering off ions without being captured; the electrons are free before the interaction and remain free afterwards.



rays but bright in neutrinos [161].

Present detection rates suggest that low-luminosity GRBs with mildly relativistic outflows, like GRB 060218, are two orders of magnitude more common than conventional GRBs [162, 163]. In addition, mildly relativistic jets are supposed to be more baryon rich. Thus, their contribution to the neutrino background could be even larger than conventional high-luminosity GRBs [164, 165].

Neutrino production in GRBs depends on the Doppler factor of the blast wave and the baryon load related to the energy contribution of nonthermal protons <sup>9</sup>. Provided that the baryon-loading factor is well above 10 and the Doppler factor is  $\leq 200$ , as required to produce ultra high-energy cosmic rays in the framework of the collapsar model, neutrinos from GRBs might be detectable with IceCube [160].

Given that particle acceleration up to energies well above the TeV scale must take place in TeV blazars, it is assumed they are the most probable neutrino sources. However it is more likely that the so-called flat spectrum radio blazars are brighter neutrino sources [130]. The reason is that some flat spectrum radio quasars (FSRQs) attain fluxes ten times brighter than the TeV (BL Lac) blazar fluxes. In fact, the absence of TeV radiation in FSRQs could be just a consequence of opacity, i.e.  $\gamma\gamma$  attenuation with the extragalactic photon background or its own accretion disc radiation. In a conservative analysis it has been shown that IceCube could detect one or several neutrinos during bright FSRQ blazar flares, such as that observed from 3C 279 in 1996 [167].

## ACKNOWLEDGMENTS

The author is grateful to G.E. Romero for a critical reading of the manuscript and useful remarks, and M.M. Reynoso for fruitful discussions about emission processes in XRBs. Thanks are also due to FUNCAP (Brazil) for financial support.

## REFERENCES

1. G. E. Romero, H. R. Christiansen and M. Orellana, *Astrophys. J* **632**, 1093 (2005).
2. G. E. Romero, *Chin. J. Astron. & Astrophys. Supp. Proc.* **5** p. 110–120 (2005).
3. M. Orellana, P. Bordas, V. Bosch-Ramon, G. E. Romero, J. M. Paredes, *Astron. & Astrophys.* **476**, 9 (2007).
4. B. Cerutti, G. Dubus, G. Henri, 2009, arXiv:0909.5587.
5. H. R. Christiansen, M. Orellana and G. E. Romero, *Phys. Rev. D* **73** 063012 (2006).
6. M. M. Reynoso, G. E. Romero, H. R. Christiansen, *Mon. Not. R. Astron. Soc.* **387**, 4, 1745 (2008).
7. Q. Z. Liu, J. van Paradijs, E. P. van den Heuvel, *Astron. & Astrophys.* **469** 807–810 (2007).
8. Q. Z. Liu, J. van Paradijs, E. P. van den Heuvel, *Astron. & Astrophys.* **455** 1165–1168 (2006).
9. M. Del Santo, J. Malzac, E. Jourdain, T. Belloni, P. Ubertini, *Mon. Not. R. Astron. Soc.* **390**, 227 (2008).
10. J. Malzac and R. Belmont, *Proc. VII Microquasar Workshop: Microquasars and Beyond*. September 1 - 5, 2008. Foca, Izmir, Turkey. PoS 2008. arXiv:0810.4589.

---

<sup>9</sup> It has been argued that with the exception of the signal originating in an initial 'proper' gamma-ray burst, all the other spikes and time variabilities can be explained by the interaction of the accelerated-baryonic-matter pulse with inhomogeneities in the interstellar matter [166].

11. R. A. Sunyaev, L. G. Titarchuk, *Astron. & Astrophys.* **86**, 121 (1980).
12. J. Homan et al., *ApJS* **132**, 377 (2001).
13. R. P. Fender, T. M. Belloni, E. Gallo, *Mon. Not. R. Astron. Soc.* **355**, 1105 (2004).
14. T. Belloni et al., *Astron. & Astrophys.* **440**, 207 (2005).
15. E. G. K rding, S. Jester, R. Fender, *Mon. Not. R. Astron. Soc.* **372**, 1366 (2006).
16. C. Done, M. Gierlinski, A. Kubota, *Astron. & Astrophys. Rv* **15**, 1 (2007).
17. A. A. Galeev, R. Rosner, G. S. Vaiana, *Astrophys. J.* **229**, 318 (1979).
18. A. A. Zdziarski, J. Poutanen, W. S. Paciesas, L. Wen, *Astrophys. J.* **578**, 357 (2002).
19. R.P. Fender et al., *Mon. Not. R. Astron. Soc.* **519**, L165 (1999).
20. N. I. Shakura, R. A. Syunyaev, *Astron. & Astrophys.* **24**, 337 (1973).
21. A. A. Esin, J. E. McClintock, R. Narayan, *Astrophys. J.* **489**, 865 (1997).
22. J. Poutanen, J. H. Krolik, F. Ryde, *Mon. Not. R. Astron. Soc.* **292**, L21 (1997).
23. R. D. Blandford, M. C. Begelman, *Mon. Not. R. Astron. Soc.* **303**, L1 (1999).
24. S. Markoff, M. A. Nowak and J. Wilms, *Astrophys. J.* **635** 1203 (2005).
25. T. J. Maccarone, *Mon. Not. R. Astron. Soc.* **360** L68 (2005).
26. R. P. Fender, *Mon. Not. R. Astron. Soc.* **322**, 31 (2001).
27. S. Corbelet et al., *Astron. & Astrophys.* **400**, 1007 (2003).
28. E. Gallo, R.P. Fender, G.G. Pooley, *Mon. Not. R. Astron. Soc.* **344**, 60 (2003).
29. A. Merloni, S. Heinz, T. Di Matteo, *Mon. Not. R. Astron. Soc.* **345**, 1057 (2003).
30. H. Falcke, E. K rding, S. Markoff, *Astron. & Astrophys.* **414**, 895 (2004).
31. I. F. Mirabel, in T. Belloni (ed.): *The Jet Paradigm, From Microquasars to Quasars, Lect. Notes Phys.* **794** (2009). arXiv:0805.2378
32. S. Corbel et al., *Science* **298**, (2002) 196.
33. V. Bosch-Ramon, *Astrophys. Space Sci.* **309**, 321 (2007).
34. J. Ferreira, P. O. Petrucci, G. Henri, L. Saug  and G. Pelletier, *Astron. & Astrophys.* **447** 813 (2006).
35. M. V. Barkov and S. S. Komissarov, *Mon. Not. R. Astron. Soc.* **385** 28 (2008).
36. H.C. Spruit, in Belloni, T. (ed.): *The Jet Paradigm - From Microquasars to Quasars, Lect. Notes Phys.* **794** (2009). arXiv:0804.3096.
37. G.S. Bisnovatyi-Kogan, A.A. Ruzmaikin, *Ap. Space Sci.* **42**, 401 (1976).
38. R.D. Blandford, D.G. Payne, *Mon. Not. R. Astron. Soc.*, 199, 883 (1982).
39. G.I. Ogilvie, M. Livio, *Astrophys. J.* **553**, 158 (2001).
40. T. Kotani, N. Kawai, T. Aoki, et al., *PASJ* **46**, L147 (1994).
41. T. Kotani, N. Kawai, M. Matsuoka, W. Brinkmann, *PASJ* **48**, 619 (1996).
42. S. Migliari, R. Fender, M. M ndez, *Science* **297**, 1673 (2002).
43. E. Gallo, et al., *Nature* **436**, 819 (2005).
44. S. Heinz, *Astrophys. J.* **636**, 316 (2006).
45. M.J. Rees, M.C. Begelman, R.D. Blandford et al., *Nature* **295**, 17 (1982).
46. X. Chen, M.A. Abramowicz, J.-P. Lasota et al., *Astrophys. J.* **443**, L61 (1995).
47. R.E. Rutledge et al., *Astrophys. J.S* **124**, 265 (1999).
48. T. Belloni, J. Homan, P. Casella et al., *Astron. & Astrophys.* **440**, 207 (2005).
49. J. Homan, T. Belloni, *Ap&SS* **300**, 107 (2005).
50. H.C. Spruit, D.A. Uzdensky, *Astrophys. J.* **629**, 960 (2005).
51. G. Drenkhahn, *Astron. & Astrophys.* **387**, 714 (2002).
52. D. Giannios, H.C. Spruit, *Astron. & Astrophys.* **450**, 887 (2006).
53. W. Brinkmann et al., *Astron. & Astrophys.* **463**, 611-619 (2007).
54. V. Bosch-Ramon and D. Khangulyan, *Int. J. Mod. Phys. D* **18**, 347-387 (2009).
55. S. Zenitani and M. Hoshino, *Astrophys. J.* **562**, 63 (2001).
56. A. Neronov and F. A. Aharonian, *Astrophys. J.* **671**, 85 (2007).
57. F. Rieger and F. A. Aharonian, *Astron. & Astrophys.* **479**, L5 (2008).
58. E. V. Derishev, F. A. Aharonian, V. V. Kocharovsky and V. V. Kocharovsky, *Phys. Rev. D* **68**, 3003 (2003).
59. B. Stern and J. Poutanen, *Mon. Not. R. Astron. Soc.* **372**, 1217 (2006).
60. M. Gierlinski and C. Done, *Mon. Not. R. Astron. Soc.* **342**, 1083 (2003).
61. S. Markoff, H. Falcke and R. Fender, *Astron. & Astrophys.* **372**, 25 (2001).
62. V. Bosch-Ramon and J. M. Paredes, *Astron. & Astrophys.* **417**, 1075 (2004).
63. G. E. Romero, M. M. Kaufman Bernad  and I. F. Mirabel, *Astron. & Astrophys.* **393**, 61 (2002).

64. M. Georganopoulos, F. A. Aharonian and J. G. Kirk, *Astron. & Astrophys.* **388**, 25 (2002).
65. R.J. Protheroe, *Topics in Cosmic-rays Astrophysics*, vol 230, Ed. M.A Du Vernois, Nova Sci. Pub. Commack NY 1999, p.247, arxiv:9812055.
66. M. Perucho and V. Bosch-Ramon, *Astron. & Astrophys.* **482**, 917 (2008).
67. J. M. Paredes, V. Bosch-Ramon and G. E. Romero, *Astron. & Astrophys.* **451**, 259 (2006).
68. V. Bosch-Ramon, G. E. Romero and J. M. Paredes, *Astron. & Astrophys.* **447**, 263 (2006).
69. A. M. Atoyan and F. A. Aharonian, *Mon. Not. R. Astron. Soc.* **302**, 253 (1999).
70. C. Dermer and M. Böttcher, *Astrophys. J.* **643**, 1081 (2006).
71. J. M. Paredes, M. Ribó and J. Martí, *Astron. & Astrophys.* **393**, 99 (2002).
72. M. M. Kaufman Bernadó, G. E. Romero and I. F. Mirabel, *Astron. & Astrophys.* **385**, 10 (2002).
73. D. Khangulyan, F. Aharonian and V. Bosch-Ramon, *Mon. Not. R. Astron. Soc.* **383**, 467 (2008).
74. G. E. Romero, D. F. Torres, M. M. Kaufman Bernadó and I. F. Mirabel, *Astron. & Astrophys.* **410**, 1 (2003).
75. A. Levinson and E. Waxman, *Phys. Rev. Lett.* **87**, 171101 (2001).
76. F. Aharonian, in *Int. Conf. Neutrino Physics and Astrophysics* (2006), arXiv:astro-ph/0702680.
77. W. Bednarek, *Astrophys. J.* **631**, 466 (2005).
78. F. M. Rieger, V. Bosch-Ramon and P. Duffy, *Astrophys. Space Sci.* **309**, 119 (2007).
79. H. van der Laan, *Nature* **211**, 1131 (1966).
80. C. R. Kaiser and P. Alexander, *Mon. Not. R. Astron. Soc.* **286** 215 (1997).
81. S. Heinz and R. Sunyaev, *Astron. & Astrophys.* **390**, 751 (2002).
82. P. Bordas, V. Bosch-Ramon and J. M. Paredes, *Int. J. Mod. Phys. D* **17** 1895 (2008).
83. S. Migliari, *The Complete Spectrum of a Compact Jet from a Neutron Star X-Ray Binary* AIP Conf. Proc. May 23, 2008, Volume 1010, pp. 23–29.
84. S. Migliari, R. P. Fender, *Mon. Not. R. Astron. Soc.* **366**, 79 (2006).
85. S. Migliari et al., *Mon. Not. R. Astron. Soc.* **351**, 186 (2004).
86. M. Massi, M. Kaufman Bernadó, *Astron. & Astrophys.* **477** 1 (2008).
87. R. P. Fender and M. A. Hendry, *Mon. Not. R. Astron. Soc.* **317**, 1 (2000).
88. D. L. Meier, S. Koide, and Y. Uchida, *Science* **291**, 84 (2001).
89. L. G. Titarchuk, C. F. Bradshaw, K. S. Wood, *Astrophys. J.* **560**, 55 (2001).
90. S. Migliari, et al., *Astrophys. J.* **643**, L41 (2006).
91. D. M. Russell, R. P. Fender, P. G. Jonker, *Mon. Not. R. Astron. Soc.* **379**, 1108 (2007).
92. F. A. Aharonian, et al. (HESS Coll.), *Science* **309**, 746 (2005).
93. F. A. Aharonian, et al. (HESS Coll.), *Science* **314**, 1424 (2006).
94. J. Albert, et al. (MAGIC coll.), *Science* **312**, 1771 (2006).
95. J. Albert, et al. (MAGIC coll.), *Astrophys. J.* **665**, L51 (2007).
96. V. Acciari, et al. (VERITAS coll.), *Astrophys. J.* **679**, 1427 (2008).
97. R. C. Hartman, et al., *Astrophys. J. Sup. Ser.* 123, 79–202 (1999).
98. A. Giuliani, et al., *5th Science AGILE Workshop*, 12–13 June (2008), Tor-Vergata, ESRIN.
99. M. M. Reynoso, H. R. Christiansen and G. E. Romero, *Astropart. Phys.* **28** 565, (2008).
100. T. Y. Saito, et al. (for the MAGIC coll.), *Procs. of the 31st ICRC*, Lodz (2009), arXiv 0907.1017.
101. J. Albert, et al., (MAGIC collaboration), *Astrophys. J.* **693**, 303 (2009).
102. P. Esposito, et al., *Astron. & Astrophys.* **474**, 575 (2007).
103. J. M. Paredes, in *IV Heidelberg International Symposium on High Energy Gamma-Ray Astronomy* (2008), arXiv:0810.4428v1.
104. W. Bednarek, & Giovannelli, F., *Astron. & Astrophys.* **464**, 437 (2007).
105. A. Abdo, et al. (FERMI Lat coll.) *Astrophys. J.* **701** L123–127 (2009).
106. J.M. Paredes, *Int. J. Mod. Phys. D* **17**, 1849 (2008).
107. L. Dessart, S.P. Owocki, *Astron. & Astrophys.* **406**, L1 (2003).
108. J. Puls, et al., *Astron. & Astrophys.* **454**, 625 (2006).
109. S.P. Owocki, G. E. Romero, R. H. D. Townsend, and A. T. Araudo, *Astrophys. J.* 2009, arXiv:0902.2278.
110. I. F. Mirabel, et al., *Astron. & Astrophys.* **330**, L9 (1998).
111. A. P. Marscher, et al., *Nature* **417**, 625 (2002).
112. C. D. Dermer, in *Procs. TeV Particle Astrophysics II Workshop*, *J. Phys. Conf. Series* **60** 8–13 (2007), arXiv:astro-ph/0611191.
113. A. Karle et al., *Nuc. Phys. B (Proc. Suppl.)* **118**, 388 (2003).

114. C. D. Dermer and A. Atoyan *New J. Phys.* **8**, 122 (2006).
115. J. M. Paredes, J. Martí, M. Ribó, and M. Massi, *Science* **288**, 2340 (2000).
116. D. F. Torres and F. Halzen, *Astropart. Phys.* **27**, 500 (2007).
117. A. Neronov, M. Ribordy, *Phys. Rev. D*, **79**, (2009) 043013.
118. R. Abbasi, et al. (ICECUBE collaboration), *Astrophys. J. Lett.* **701**, pp. L47–L51 (2009).
119. V. Van Elewyck, (for the ANTARES collaboration), arXiv:0908.2454 (2009).
120. C. Distefano (for the NEMO collaboration), *Nucl. Phys. B (Proc. Suppl.)* **165**, 181–187 (2007). S. Aiello, et al. (NEMO collaboration), *Astropart. Phys.* **28**, 1–9 (2007).
121. R. M. Hjellming, K. J. Johnston, *Astrophys. J.* **328**, 600 (1988).
122. E.G. Körding, R. P. Fender, S. Migliari, *Mon. Not. R. Astron. Soc.* **369**, 1451 (2006).
123. M.C. Begelman, B. Rudak, M. Sikora, *Astrophys. J.* **362**, 38 (1990).
124. J.H. Krolik, in *Active Galactic Nuclei*. Princeton University Press, Princeton 1999.
125. S. Komissarov, M. Barkov, N. Vlahakis, A. Königl, *Mon. Not. R. Astron. Soc.* **380**, 51 (2007).
126. G. Ghisellini, L. Maraschi, A. Treves, *Astron. & Astrophys.* **146**, 204 (1985).
127. M. M. Reynoso, G. E. Romero, *Astron. & Astrophys.* **493**, pp.1–11 (2009).
128. G. E. Romero, G. S. Vila, *Astron. & Astrophys.* **485**, 623 (2008).
129. G. R. Blumenthal, R. J. Gould, *Rev. Mod. Phys.* **42**, 237 (1970).
130. A. M. Atoyan, C. D. Dermer, *Astrophys. J.* **586**, 79 (2003).
131. A. M. Cherepashchuk et al., *Astron. & Astrophys.* **437**, 561 (2005).
132. D. R. Gies et al., *Astrophys. J.* **566**, 1069 (2002).
133. S. R. Kelner, F. A. Aharonian, *Phys. Rev. D* **78**, 034013 (2008).
134. S. R. Kelner, F. A. Aharonian, V. V. Bugayov, *Phys. Rev. D* **74**, 034018 (2006).
135. D. Khangulyan, S. Hnatic, F.A. Aharonian, S. Bogovalov, *Mon. Not. R. Astron. Soc.* **380**, 320 (2007).
136. A. T. Araudo, V. Bosch-Ramon, G. E. Romero, *Astron. & Astrophys.* **503**, 673 (2009).
137. G. S. Vila and G. E. Romero, 2009 *Leptonic/hadronic models for electromagnetic emission in microquasars: the case of GX 339-4*, submitted.
138. T. K. Gaisser, 1990, *Cosmic Rays and Particle Physics*, Cambridge University Press, Cambridge.
139. P. Lipari, M. Lusignoli, D. Meloni, *Phys. Rev. D* **75**, 123005 (2007).
140. F. Halzen, *Eur. Phys. J. C* **46**, 669–687 (2006).
141. S. Aiello et al., *Astroparticle Phys.* **28**, 1 (2007).
142. A. T. Araudo, G. E. Romero, V. Bosch-Ramon and J. M. Paredes, *Int. J. Mod. Phys. D* **17** 1889–1894 (2008).
143. F. Aharonian, et al., *Astron. & Astrophys.* **393**, L37–L40 (2002).
144. F. Aharonian et al., *Astron. & Astrophys.* **467**, 1075–1080 (2007).
145. R. Chavez, *IV Heidelberg Int. Symposium on High Energy Gamma-Ray Astronomy* (2008).
146. J. Martí, L. F. Rodríguez, and B. Reipurth, *Astrophys. J.* **449**, 184–187 (1995).
147. P. Benaglia, and G. E. Romero, *Astron. & Astrophys.* **399**, 1121–1134 (2003).
148. W. Bednarek, *Mon. Not. R. Astron. Soc.* **382**, 367–376 (2007).
149. D. Eichler, and V. Usov, *Astrophys. J.* **237**, 236–243 (1993).
150. P. Benaglia, G. E. Romero, B. Koribalski, and A. M. T. Pollock, *Astron. & Astrophys.* **440**, 743–750 (2005).
151. J.M. Pittard, S. M. Dougherty, *Mon. Not. R. Astron. Soc.* **372**, 801–826 (2006).
152. E. Parizot, A. Marcowith, E. van der Swaluw, A. Bykov, V. Tatischeff, *Astron. & Astrophys.* **424**, 747–760 (2004).
153. P. Sreekumar, et al., *Astrophys. J.* **400**, L67–L70 (1992).
154. A. Loeb and E. Waxman *J. Cosmology Astropar. Phys.* **5**, 3 (2006).
155. P. Mészáros, *Rep. Prog. Phys.* **69**, 2259 (2006).
156. S. E. Woosley, *Astrophys. J.* **405**, 273 (1993).
157. E. Waxman and J. N. Bahcall, *Phys. Rev. Lett.* **78**, 2292 (1997).
158. J. Alvarez-Muniz, F. Halzen, and D.W. Hooper, *Phys. Rev. D* **62**, 093015 (2000).
159. E. Waxman and J. N. Bahcall, *Astrophys. J.* **541**, 707 (2000).
160. C. D. Dermer and A. Atoyan, *Phys. Rev. Lett.* **91**, 071102 (2003).
161. P. Mészáros and E. Waxman, *Phys. Rev. Lett.* **87**, 171102 (2001).
162. S. Campana et al., *Nature (London)* **442**, 1008 (2006).
163. E. Waxman, P. Mészáros, and S. Campana, *Astrophys. J.* **667**, 351 (2007).

- 164. N. Gupta and B. Zhang, *Astropart. Phys.* **27**, 386 (2007).
- 165. S. Ando and J. F. Beacom, *Phys. Rev. Lett.* **95**, 061103 (2005).
- 166. R. Ruffini et al., *Nuovo Cim. B* **116** 99–108 (2001).
- 167. A. Atoyan and C. D. Dermer, *Phys. Rev. Lett.* **87**, 211102-1 (2001).